 doi:10.20944/preprints202208.0069.v1

Article

Novel Synthesis Methods of New Imidazole-Containing Coordination Compounds and Salts Tc(IV, V, VII) – Reaction Mechanism, XRD and Hirshfeld Surface Analysis

Mikhail Alexandrovich Volkov*, Anton Petrovich Novikov, Mikhail Semenovich Grigoriev, Alexander Mikhailovich Fedoseev and Konstantin Eduardovich German

Frumkin Institute of Physical Chemistry and Electrochemistry, Russian Academy of Sciences, Leninskii prospect 31-4, 119071 Moscow, Russia; tony.novickoff@yandex.ru (A.P.N.); mickgrig@mail.ru (M.S.G.); a.fedosseev@gmail.com (A.M.F.); guerman_k@mail.ru (K.E.G.)

* Correspondence: mikhailalexvol@gmail.com

Abstract: In this work, we have proposed two new methods for the synthesis of $[TcO_2L_4]^+$ (where L = imidazole (Im), methylimidazole (MeIm)) complexes using thiourea (Tu) and Sn(II) as reducing agents. The main and by-products of the reactions were determined, and possible reaction mechanisms were proposed. We have shown that the reduction of Tc(VII) with thiourea is accompanied by the formation of the Tc(III) intermediate and further oxidation to Tc(V). The reaction conditions changing can lead to the formation of Tc(VII) and Tc(IV) salts. Seven new crystal structures are described in this work: Tc(V) complexes, salts with Tc(VII) and Tc(IV) anions. For halide salts of Tu the cell parameters were determined.

In all obtained compounds, except for $[TcO_2(MeIm)_4]TcO_4$, there are π-stacking interactions between aromatic rings. An increase in the anion size lead to weaken intermolecular interactions. Halogen bonds and anion-π interactions have also been found in hexahalide-containing compounds. The Hirshfeld surface analysis showed that the main contribution to the crystal packing is made by van der Waals interactions of the H···H type (42.5–55.1%), H···C/C ···H (17.7–21.3%) and hydrogen bonds, which contribute 15.7–25.3% in total.

Keywords: technetium; imidazole; technetyl; XRD-analysis; Hirshfeld surface analysis; π-interactions; metal-nitrogen bond; supramolecular chemistry

1. Introduction

Technetium is mostly chemically and environmentally available as an $Tc(VII)O_4^-$ and therefore in most reactions possess oxidative properties. Depending on the reducing conditions and the chemical nature of the ligand available, $Tc(VII)O_4^-$ may convert to stable/unstable final/intermediate species of Tc(V), Tc(VI) or Tc(III). Under very special conditions the products could be either cluster nature [1] or carbonyl derivatives [2,3] of Tc[2+, 2.5+ and 0] oxidation states. Very high attention is focused at Tc(V) and Tc(III) complexes that play important role in preparative [4–6], radiopharmaceutical [7,8] and industrial reprocessing chemistry of Tc [9].

Weak, intermolecular interactions are of particular interest from a theoretical point of view, the study of which in pertechnetates and perrhenates of purines led to the discovery of a new type of chemical bond [10]. New methods of separating perrhenates and pertechnetates are based on non-valent interactions [11–14]. The study of the non-valent interactions contribution for various technetium compounds will allow a deeper understanding of the impact of radiopharmaceuticals on living organisms [7], of the formation of non-trivial technetium complex compounds, similar to those described in [4,5,15]. Information about weak interactions can also be useful for predicting the behavior of Tc-

containing intermediates in catalytic and sorption processes on complex organic sorbents like those described[16].

Halide systems have now received a new meaning for high-temperature pyrometallurgical reprocessing of spent nuclear fuel. One approach to this is the use of low-temperature melts and ionic liquids based on imidazole derivatives. It is known that concentrated hydrohalogen acids form stable compounds $TcO(Hal)_4^{2-}$, but during its long-term storage, Tc(V) transforms into hexahalide compounds of Tc(IV). However, with the presence of ligands in Tc(V) solutions, it becomes possible to obtain useful functional complexes, which was shown in the work [17]. There is no description in the literature of Tc(IV) hexahalide complexes with imidazolium cations. In the course of operation of molten-salt reactors, $TcHal_6^{2-}$ compounds will inevitably accumulate. The study of the crystal structure, intermolecular interactions, and conditions for the formation of technetium hexahalides can be used to develop methods for reprocessing fuel for new types of reactors [18,19]. It should be taken into account that $TcHal_6^{2-}$ compounds can be used to purify and obtain metallic technetium, which is considered the most acceptable form for long-term storage or transmutation of technetium.

The reduction of pertechnetate ions with organosulfur compounds (inorganic Na2S2O3 or organic thiourea (Tu)) leads to the formation of Tc(V) [20,21] depending on the present ligands, which the authors of the following work pay attention to [22].

In Fackler and co-workers in 1985 [1] the structure of $[TcO_2(Im)_4]Cl{\cdot}2H_2O$ (Im = imidazole) was analyzed. The Tc=O distances were used in some databases as reference for TcO_2^+ giving an idea of large variation of Tc=O in technetyl cation – the observation being in fact erroneous due to initial misinterpretation of the space group in the compound structure. Meanwhile, the great interest to technetyl(V) derivatives arose due to the account that its application in nuclear medicine as biologically active ^{99m}Tc radiopharmaceuticals is based on Tc(V) formation with $[O=Tc=O]^+$ as a complex forming center [23–26]. The Tc complexes of such type with amine and imine ligands are the principle models for Tc bounding to aminoacids, proteins, antibodies etc. In general, Tc (V) forms usually trans -$[O_2L_4Tc]^+$, where L is N-bearing organic ligand [17]. Imidazole rings are often found in biochemical systems applicable to metal coordination.

The R-factor obtained in [17] for $[TcO_2(Im)_4]Cl \cdot 2H_2O$, was equal to 0.091 with the abnormally short distances Tc–O, that are characteristic more of Tc(VII), then of Tc(V). Analyses of local symmetry and the *hkl* set support the erroneous interpretation of the space group to centrosymmetric one by the authors of [17] for the structure $[TcO_2(Im)_4]Cl{\cdot}2H_2O$. Nowadays a great database for metalloyl cations complexes is available, and the typical tendencies indicate that the structure of $[TcO_2(Im)_4]Cl{\cdot}2H_2O$ in [17] was confusing, we considered reasonable to undertake new research of its analogues with the principle idea to enlarge (and possibly to correct) the database for technetyl complex compounds and its' structural understanding.

The paper considers a new method for the preparation of $[TcO_2(R\text{-}Im)_4]X$ (X = Br, TcO_4, R = Me, H) compounds, their crystal structures are studied, non-valence interactions are analyzed by the Hirshfeld surfaces method and IR spectroscopy of $[TcO_2(Im)_4]Br{\cdot}2H_2O$. A detailed analysis of the reactional by-products was carried out and new imidazole complexes Tc(VII) and Tc(IV) were identified, the optimal conditions for the formation of the complex-forming nucleus TcO_2^+ by the proposed method were determined.

2. Results and discussion

2.1. Structural Description of Tc(V) complexes

Compounds I-IV contain $[TcO_2L_4]^+$ cationic complexes, in which the Im (MeIm) molecules are coordinated to the Tc atom by the N atom (Fig.1). Crystal structure data for the compound **I** were obtained from [17]. The $[TcO_2Im_4]Cl{\cdot}2H_2O$ structure described earlier in the centrosymmetric space group *C2/c* with disordering of the chloride ion and water

molecules is, probably, not centrosymmetric and similar to **II**. The oxygen atoms are in the trans-position (the angles O-Tc-O are close to 180º) The N-Tc-N angles are close to 90º in all complexes (Tables S2, S6, S10). In **II**, three imidazole rings are turned in one direction (C1, C7 and C10 atoms on one side of the equatorial plane of the TcO_2 group), and only one ring is turned in the other direction (C4 on the other side of the plane) (Figure 1). In structures **III** and **IV**, the opposite imidazole rings are turned in different directions. Although in all structures the imidazole rings are planar, they are not parallel to the O···O direction. In structure **II**, the two opposite rings are rotated more away from this direction (torsion angles O1-Tc1-N1-C3 and O1-Tc1-N3-C4 are 159.1º and 164.2º, respectively), than the others two (the torsion angles O1-Tc1-N7-C12 and O1-Tc1-N5-C8 are 170.1º and 175.4º). In **III**, the imidazole rings deviate more strongly from the O···O direction (torsion angles change from 150º to 155º), while in **IV**, on the contrary, they are close to this direction (torsion angles change from 168.1º to 175.0º).

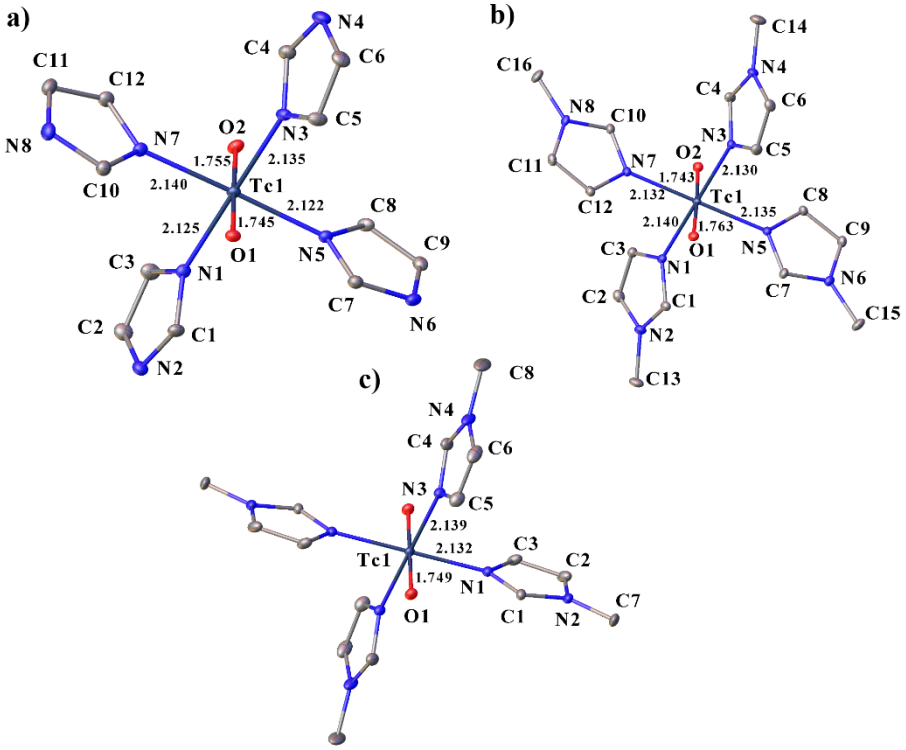

Figure 1. Molecular structure of **II (a)**, **III (b)** and **IV (c)** showing the coordination of the technetium atom with some bond lengths and labeling. Solvent molecules, counterions and H-atoms are omitted for clarity.

The Tc–N distances in all complexes are approximately equal and change from 2.122 to 2.140 Å. The Tc=O distances in the complexes vary from 1.743 to 1.763 Å, which is longer than the distances described in previous works for the chlorides of these complexes [17] and used in the calculations [27].

In all structures, cations are bonded to each other through crystallization water molecules or counterions. In **II**, the cations are linked through bromide-ions by H-bonds of the N–H···Br type and through water molecules by hydrogen bonds of the N–H···O and O–H···O types. In **III**, cations are linked to water molecules by hydrogen bonds of the O–H···O type, which in turn form a water···Cl···water···water bridge to another cation. In IV, the cations are linked to each other through pertechnetate anions by weak hydrogen bonds of the C–H···O type. The crystal packing in all complexes can be represented as layered, where the molecules of the complexes form layers, between which there are molecules of anions and water (Figure 2). Additionally, the molecules of the complexes in

structure **II** are connected by two π-stacking interactions, in **III** by only one (Figure 3). The strongest π-stacking interaction is observed in structure **III** (Table 2). In structure **IV**, there are short distances between the atoms of imidazole rings, but these contacts cannot be called π-stacking [28,29] because of the large distance between the centers (4.127 Å) and the large displacement (1.944 Å) of the rings.

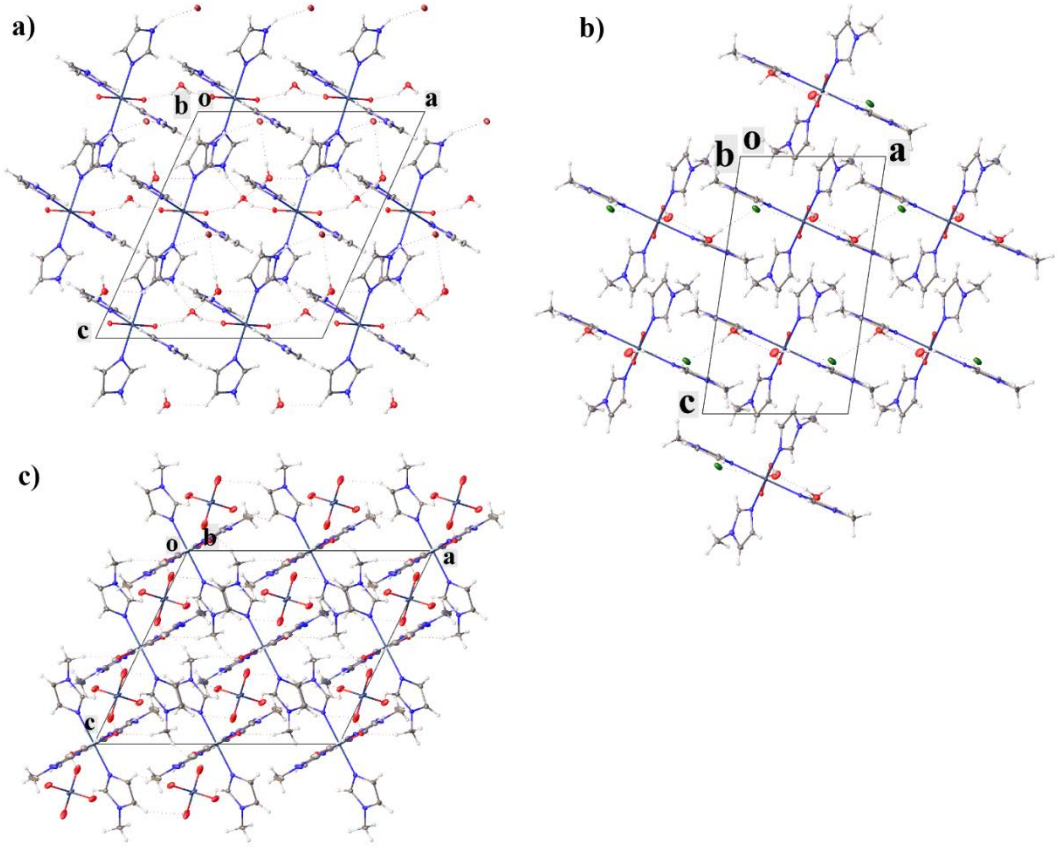

Figure 2. Crystal packing of **II (a)**, **III (b)** and **IV (c)** showing layers of complexes with solvent molecules and counterions between them. View along *b* axis.

Table 1. Parameters of π-stacking interactions.

Structure	Rings		Angle	Centroid-centroid distance	Shift distance
II	N1C3C2N2C1	N3C5C6N4C4 (symmetry code: -1/2+*x*, 1/2+*y*, *z*)	6.503	3.749	1.175
		N3C5C6N4C4 (symmetry code: -1/2+*x*, 1/2-*y*, -1/2+*z*)	5.351	3.979	1.718
III	C10N7C12C11N8	C7N5C8C9N6 (symmetry code: 1+*x*, *y*, *z*)	1.325	3.569	1.269
V	C5N1C2N3C4	C15N11C12N13C14 (symmetry code: 1-*x*, 1-*y*, 1-*z*)	4.667	3.437	1.153
	C15N11C12N13C14	C15N11C12N13C14 (symmetry code: 1-*x*, 2-*y*,1-*z*)	0.000	3.342	0.572

VI	C1N5C4C3N2	C1N5C4C3N2 (symmetry code: 2-*x*, 1-*y*, 2-*z*)	0.000	3.461	0.937
VII	C1N5C4C3N2	C1N5C4C3N2 (symmetry code: -*x*, 1-*y*, -*z*)	0.000	3.536	0.960
VIII	C6N2C7C11N1	C17N9C21C19N4 (symmetry code: *x*, 5/2 -*y* , -1/2+*z*)	3.045	3.446	1.102
	C13N8C23C20N3	C14N12C18C15N5 (symmetry code: *x*, 1+*y*, *z*)	7.555	3.532	0.892
		C14N12C18C15N5 (symmetry code: *x*, 3/2-*y*, 1/2+*z*)	6.556	3.481	1.136

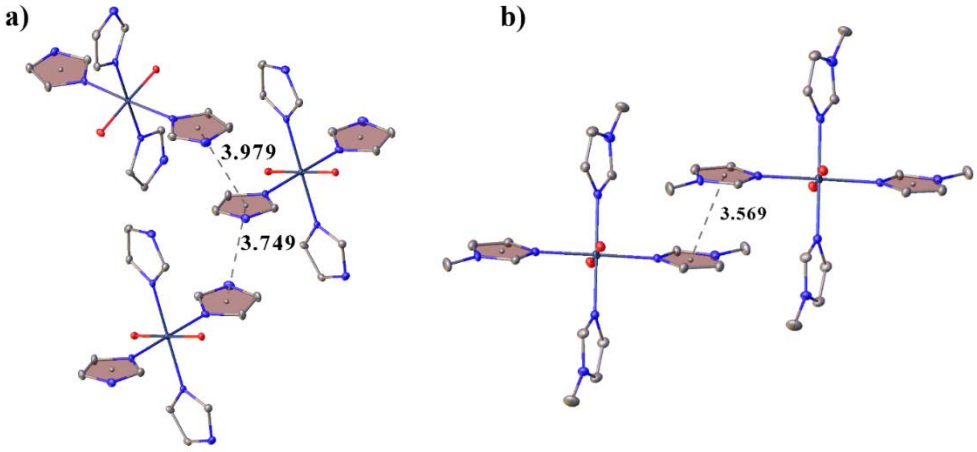

Figure 3. View showing π-stacking interactions in the structures **II (a)** and **III (b)**.

The analysis of supramolecular interactions in the obtained structures showed that an increase in the size of the anion leads to a deterioration in the binding of molecules in the crystal but does not lead to crystal packing disturbances (solvent molecules and counterions are located between the layer of cations) and suggests an increase in solubility upon passing from compound **II** to **IV**.

2.2. Structural description of by-products

Compound **V** was obtained as a by-product of the preparation of compound IV. The structure contains two MeIm molecules, one of which is protonated at the nitrogen atom, but the proton in the compound is disordered between two nitrogen atoms of different molecules (N3 and N13). The structure contains a neutral thiourea molecule and a pertechnetate-anion (Figure 4a). MeIm fragments are in the same plane (the angle between the planes is 4.67º). The crystal packing can be represented as a layered, MeIm fragments are linked to each other by a hydrogen bond of the N–H···H type into dimers and by π-stacking interaction (Table 2) into layers, as in **II**-**IV**, and pertechnetate-ions and thiourea molecules are located between the layers (Figure 4b). Thiourea molecules are linked to each other by hydrogen bonds of the N–H···S type, to pertechnetate-ions by H-bonds of the N–H···O type, and to imidazole fragments by bonds of the C–H···S type.

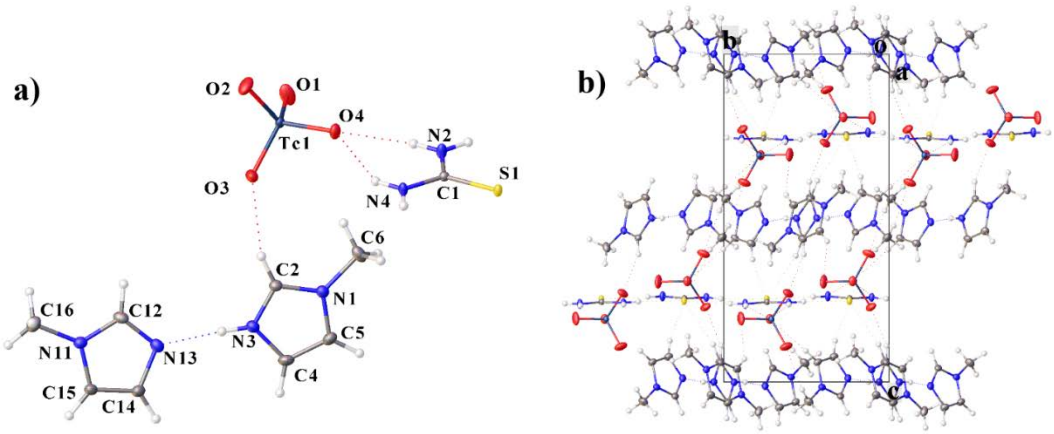

Figure 4. Molecular structure of **V** (**a**) including atom labeling and crystal packing (**b**). Only one disordered H-atom of the imidazole ring is shown.

Compounds **VI**, **VII** and **VIII** are by-products of second method. Compounds **VI** and **VII** contain protonated imidazole cations and hexahalide Tc(IV) anions (Figure 5). Compound **VIII** is a mixed salt containing 30% technetium and 70% tin in the hexahalide anion. In **VIII**, the asymmetric fragment contains four MeIm cations, the hexahalide anion, and two chloride anions. The environment of technetium or tin atoms in hexahalide anions is close to ideal octahedral (Tables S18, S23, S27).

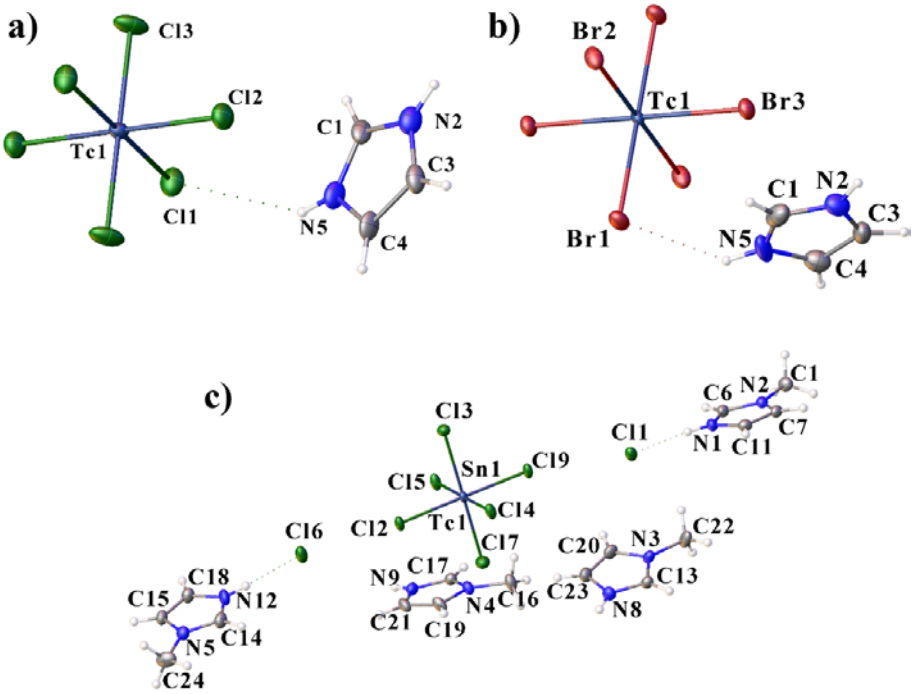

Figure 5. Molecular structure of **VI (a), VII (b)** and **VIII (c)**.

In structures **VI** – **VIII**, there are π-stacking interactions between cations (Table 2) (Figure 6). Crystal packing can be represented as layered. Cations in **VI** – **VIII** are linked into layers by π-stacking interactions, cations and anions are linked between layers by hydrogen bonds (Figure 7). In **VI** and **VII**, the anions are additionally linked by halogen bonds, and the Hal···Hal. The packing of **VI** and **VII** is very close (Figure 7), the main difference is in small rotations of anions and cations: in **VI** (sp. gr. C2/m) anions occupy a special position with symmetry 2/*m*, and cations – a special position with symmetry *m*; in

VII (sp. gr. $P2_1/c$) anions occupy a special position with symmetry -1, and cations are in a general position.

Also, in **VI – VIII** there are anion-π interaction (the distance between the center of the ring and the anion is less than 5 Å, and the angle α is greater than 50°) between hexahalide anions and imidazole rings (Figure 6) [30,31].

For compound **IX**, a crystal structure containing a dithiourea cation and chloride anions was previously described [32]. The doubly charged dithiourea cation is formed by S–S bonding of thiourea molecules. Halide anions are attached to cations by hydrogen bonds. Compound **X** is isostructural to compound **IX** (a = 8.836(1), b = 10.506(1), c = 19.695(1), sp. gr. *Pbca*), and in this paper, we determined only the crystal cell of compound **IX**: a = 9.36, b = 10.70, c = 20.17 Å, orthorombic *P*.

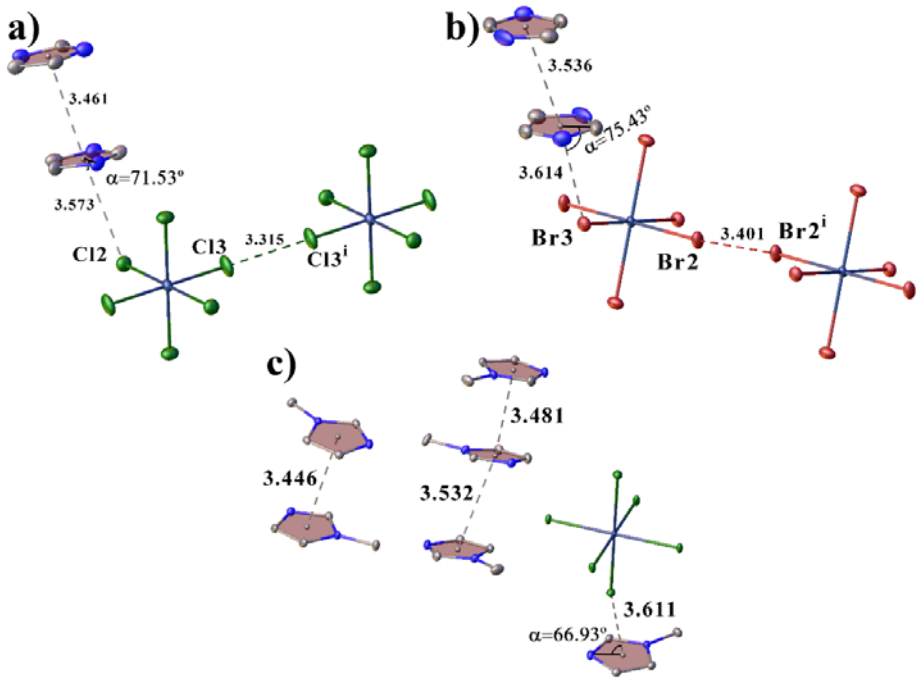

Figure 6. View showing halogen bonds, anion-π and π-stacking interactions in the structures **VI (a)**, **VII (b)** and **VIII (c)**.

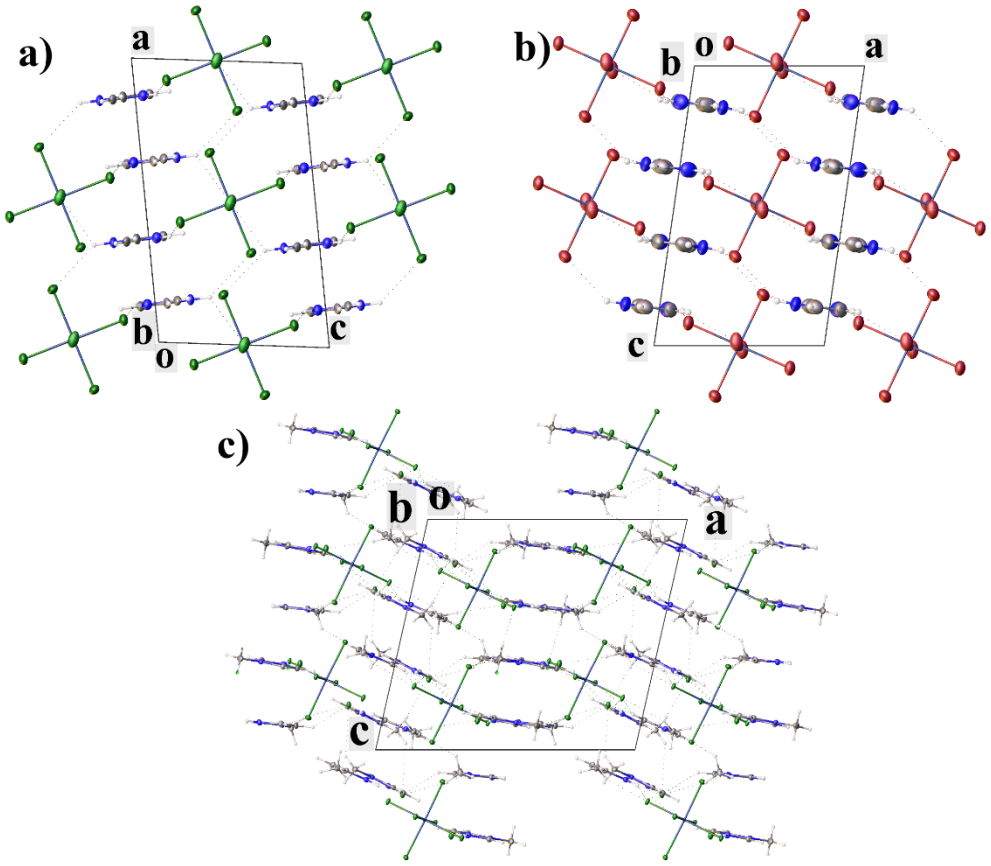

Figure 7. Crystal packing of **VI (a)**, **VII (b)** and **VIII (c)**, showing cation.

2.3. Hirshfeld Surface Analysis

Hirshfeld surface (HS) analysis is based on the division of the electron density in a crystal. The Hirshfeld surface covers the molecule and determines the volume of space in which the electron density of the promolecule exceeds the density of all neighboring molecules [33]. Fingerprint plots (2D scans of 3D surfaces) are a convenient way to analyze the intermolecular interactions present in crystals. This method can be used to analyze π-stacking interactions [34], halogen and hydrogen bonds [35,36], anion-π [28] and other weak non-covalent interactions [37,38].

The Crystal Explorer 21 [39] program was used to analyze non-valent interactions in crystals using the HS analysis. The donor-acceptor groups are visualized using a standard (high) surface resolution and d_{norm} surfaces (Figure 8a-c). Red spots on the surface of the d_{norm} plot indicate intermolecular contacts involving the hydrogen bonds. The brightest red spots correspond to the strongest hydrogen bond N—H···Hal in **II**-**III** and O–H···O in **II**. Weaker red spots correspond to C—H···Hal bonds in **II**-**III**, C—H···O in **II**-**IV** and π-stacking interactions in **II**-**III**. For additional analysis of π-stacking interactions, shape-index surfaces were described. There are π-stacking interactions in **II** and **III**, as seen from the characteristic red and blue triangles on the surface, and absent in **IV** (Figure 8d-f).

The nonvalent interactions analysis of the obtained complexes showed that the main contribution to the crystal packing is made by van der Waals interactions of the H···H type (42.5–55.1%) and H···C/C···H (17.7–21.3%). Contacts of the H···H type make the greatest contribution to III, which may be due to the appearance of a methyl group and the absence of a large number of H-bonds. A significant contribution to intermolecular interactions is made by hydrogen bonds, for which the following types are responsible: O···H/H···O and Hal···H/H···Hal, which contribute 15.7–25.3% in total. Contacts of the C···N/N···C type responsible for π-stacking interactions contribute 3.3% in **II**, 1.5% in **III**, and are practically absent in **IV** (0.1%). Contacts that contribute less than 2% are not considered in Figure 9.

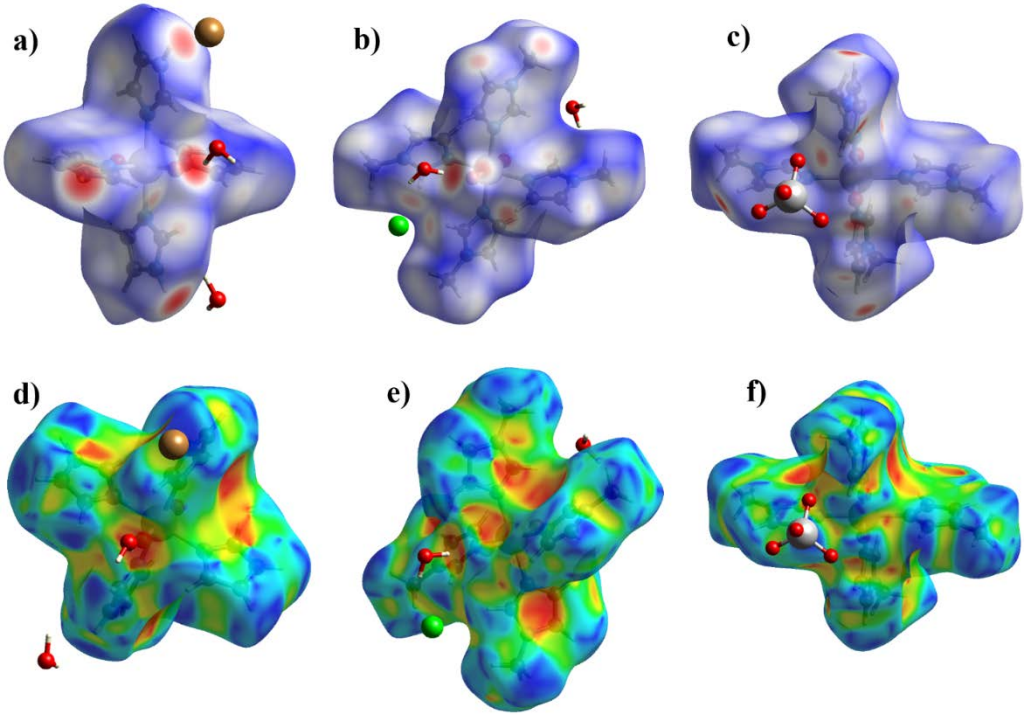

Figure 8. HS mapper over d_{norm} for **I (a)**, **II (b)**, **III (c)** and HS mapper shape-index of **I (d)**, **II (e)**, **III (f)** to visualize of intermolecular interactions in crystals.

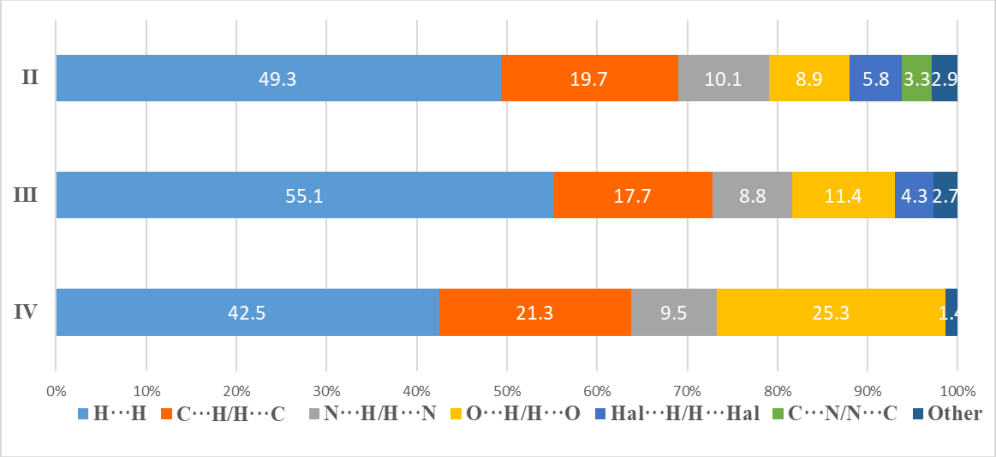

Figure 9. Percentage contributions to the Hirshfeld surface area for the various close intermolecular contacts for **II-IV**.

2.4. IR-spectroscopy

The electronic absorption spectroscopy of bright pink solutions of compounds **I** and **II** showed a broad wave with a peak of 480 ± 10 nm (Figure 10, inset), which is typical for Tc(V) compounds. Otherwise, UV-Vis spectroscopy was uninformative.

As no sulfur atoms are present in our case compound II, the group $[O=Tc=O]^+$ is completely characterized with the fluctuations bands at 790-880 cm^{-1} in infrared region [40–42]. In the IR spectrum of **II** (Figure 10) the Tc=O group is pronounced by the bands at 809.79 sm^{-1} and 847.68 cm^{-1}, (Table 3). A wide wave in the range of 2800-3700 sm-1 corresponds to the vibrations of water atoms [43] and 1500±50 sm^{-1} scissor vibrations HOH. The remaining peaks displayed on the spectrum, including those that appear in the region of 2800-3700 sm^{-1}, correspond to vibrations of carbon and nitrogen atoms in the imidazole

fragment of the compound molecule **II** [44,45]. The spectra show the peaks splitting typical for compressed tablets KBr.

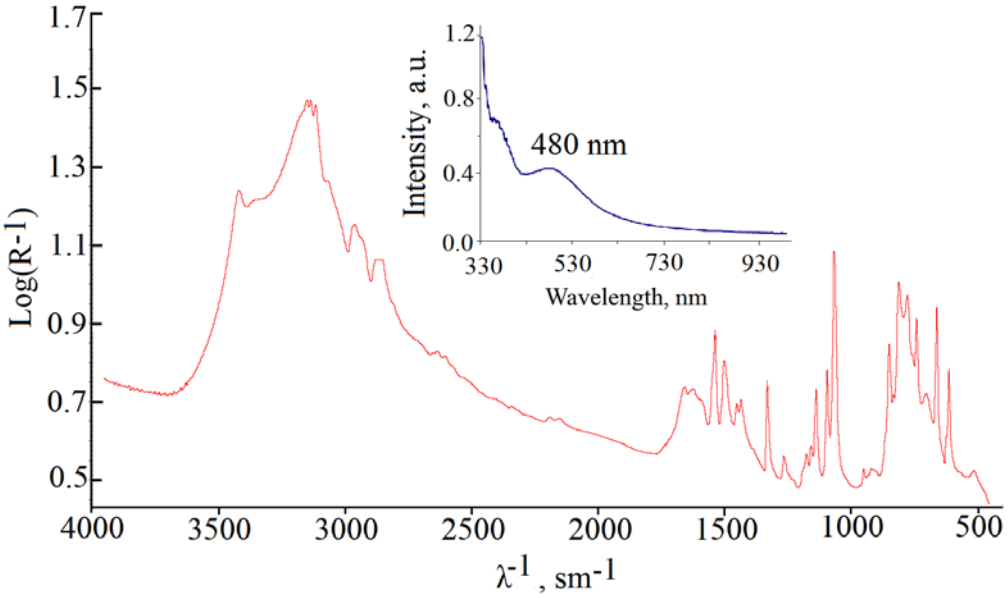

Figure 10. IR spectrum of compound **II**, inset: UV-vis spectroscopy of a methanolic solution of compound **II**.

Table 3. Absorption peaks of compound **II** in the IR spectrum.

Peak position	Intensity	Peak position	Intensity
661.82	0.915	1264.79	0.689
659.95	1.070	1330.65	0.883
739.93	1.045	1434.10	0.834
775.83	1.104	1500.61	0.934
809.79	1.134	1537.21	1.012
847.68	0.979	1655.87	0.867
1065.58	1.221	2856.37	1.192
1094.15	0.912	2961.85	1.282
1137.11	0.864	3151.49	1.605

2.5. Proposed mechanism for the formation of complexes $[TcO_2(Im)_4]^+$

The reduction reaction of pertechnetate ions with thiourea in the presence of HHal acids has a relatively low yield, but it also has advantages. The method turned out to be selective for the synthesis of $[TcO_2(R\text{-}Im)_4]^+$ complexes, and the target Tc-containing products were the only colored compounds. Changing the concentrations of thiourea and hydrohalic acid did not lead to a noticeable change in the yield of the target reaction products. Nevertheless, it should be noted that in the absence of acids (HHal or $HTcO_4$), the reaction proceeds very slowly, which can be explained as in the described compound V, where thiourea interacts with oxygen Tc=O with unprotonated nitrogen atoms of nitrogen. The experiments have shown that an excess of thiourea and an equimolar concentration of HHal acid will be optimal for the preparation of $[TcO2(R\text{-}Im)_4]^+$ compounds. An intense coloration of solutions at the first moment of the reaction manifests itself in the dissolution of Tc(III) intermediates, probably representing $[TcTu_6]^{3+}$ coordination cations described in [21]. The synthesis in an oxygen-free atmosphere hindered the formation of the target complexes; Tc(III) compounds could not be isolated in the presence of imidazoles. The combination of the above factors helped to suggest the

 doi:10.20944/preprints202208.0069.v1

mechanism for the formation of Tc(V) complexes, which is schematically presented in Figure 11.

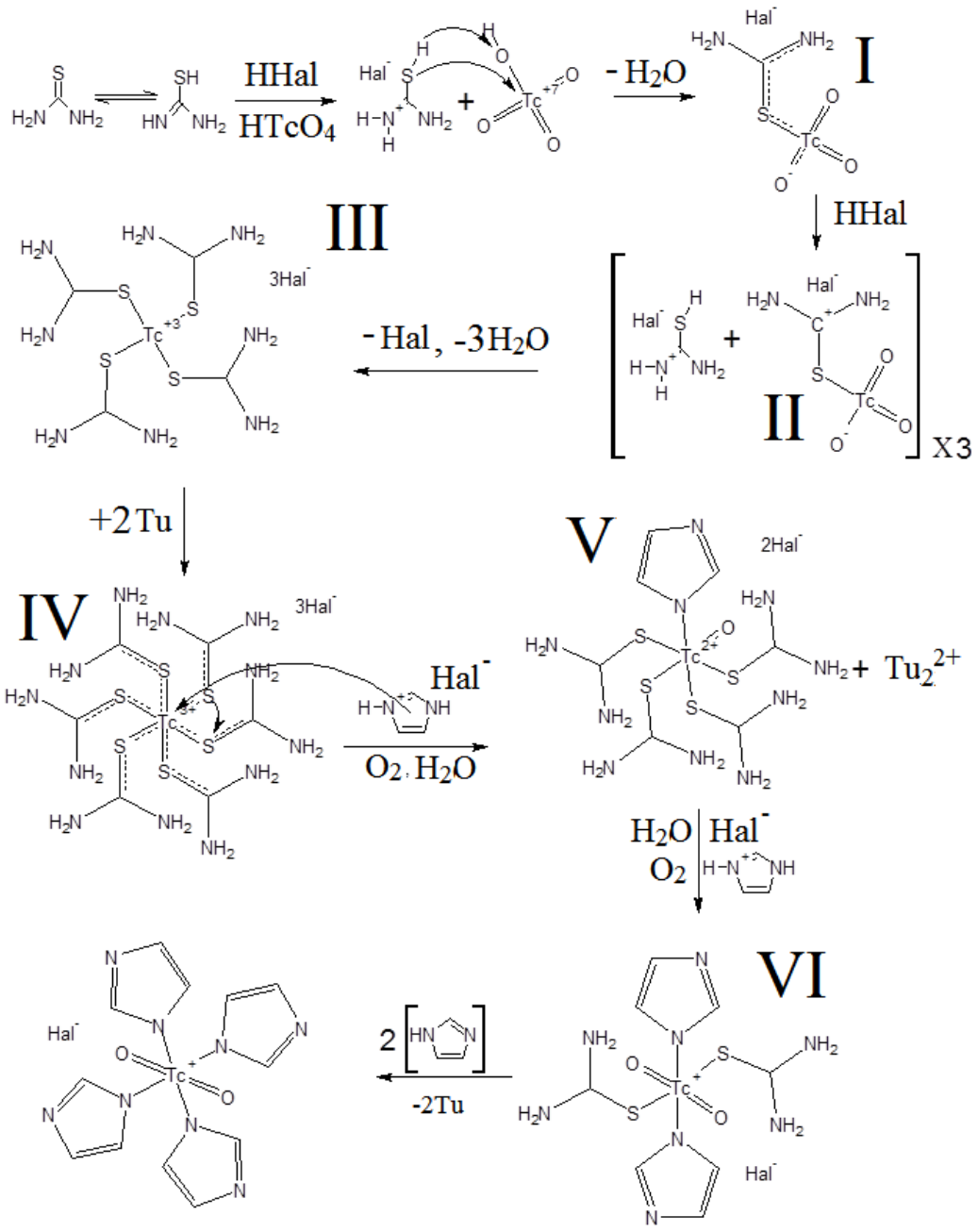

Figure 11. Proposed mechanism of Tc(VII) reduction in the presence of competitive ligands by thiourea with the formation of intermediate products.

The reduction of the pertechnetate ion and the formation of complexes apparently occur during the successive reduction of Tc(VII) to Tc(III) and subsequent oxidation with atmospheric oxygen to Tc(V). The reaction takes place in the presence of catalytic anions in an acidic medium, in which the thiol tautomeric form of thiourea is stable. The reaction begins with the SH-group reaction with the Tc-O$^-$ bond; in this case, the Tc-S bond is formed with the formation of particle I and the water molecule elimination. The redistribution of charges in an acid medium leads to an elongation of the Tc=O bond and the

formation of particle II. Repeating this process three times results in the formation of particle III. The resulting fragment is reactive and coordinates with two additional ligands, which can be assumed to contain thiourea, in the case of thiouria excess. The resulting particle IV presumably has an octahedral environment of the technetium atom [TcS_6]. The molecule of the protonated imidazolium fragment enters into a ligand exchange reaction, while the thiourea molecule leaves, taking with it the second Tu molecule with the formation of a thiourea dimer salt. A strong distortion of the geometry leads to the oxidation of technetium and the formation of the Tc-O bond, resulting in the V particle production. The reoccurrence of the substitution reaction of two Tu molecules leads to the formation of particle VI, which coordinates with two imidazole molecules and completes the coordination sphere, forming a stable reaction product $[TcO_2(Im)_4]^+$.

The mechanism of the Tc(V) complex formation reaction, according to the second proposed method, is based on the assumption of the formation of an intermediate $TcO(Hal)_5^{2-}$ particle. The ongoing hydrolysis processes lead to the formation of the $[O=Tc=O]^+$ nucleus, and in the presence of an imidazolium ligand, the final product $[TcO_2(Im)_4]^+$ is formed. A large excess of HHal acid provokes a competitive exchange of ligands; at a sufficiently high concentration, HHal reduces Tc(VII) via Tc(V) to Tc(IV) with the formation of a stable hexahalide complex.

3. Materials and Methods

Caution! ^{99}Tc is a β-emitter (A = 635 Bq/μg [46], E_{max} = 290 keV), appropriate shielding and manipulation technics were employed during the synthesis and all manipulations.

All the reagents used in the work were qualified chemically pure and were not subjected to further purification. The technetic acid used in the work was prepared by dissolving Tc_2O_7 in bidistilled water (R ≥ 18 MΩ).

*3.1 Synthesis $[TcO_2(Im)_4]Cl{\cdot}2H_2O$ (**I**), $[TcO_2(Im)_4]Br{\cdot}2H_2O$ (**II**), $[TcO_2(2\text{-}MeIm)_4]Cl{\cdot}2H_2O$ (**III**)*

Method 1

10 mg thiourea (Tu) (Merck) and 10 mg imidazole (Im) (Merck) (5 μl 2-methylimidazole (MeIm) (Merck) for compound **III**) were placed in a 1.5 ml vial and dissolved in 350 μl methanol (Sigma - Aldrich). 10 μl of 12M HCl (5M HBr for compound **II**) and 2 μl of 3.5 M $HTcO_4$ were added to the resulting solution. The vial with an intensely colored red solution was closed and left until the color changed to bright pink, then the solution was evaporated to dryness at room temperature (about 10 hours). The resulting crystalline mixtures were washed once with cold methanol (3°C), the washing solutions were colored light pink. The resulting crystals **I**, **II** and **III** were suitable for SCXRD. The compounds are infinitely soluble in alcohol, acetone, water and organic acids. Recrystallization is conveniently carried out from methanol. Approximate reaction yield of each substance by technetium: **I**, **II** ~20%, **III** ~40%.

Method 2

The compounds **I**, **II** and **III** were prepared by reduction of 100 mg $KTcO_4$ («Isotope JSC») with $SnCl_2$ (Merck) (or SnBr2 for substance II) in 1M HCl (HBr) in presence of excess Im (MeIm for substance **III**). Pink solution was formed on refluxing the reaction mixture at 80 oC for 3 hours. The pink crystals were grown on cooling and separated by filtration and recrystallized for ethanol. The mother liquors were an intense red-brown color. The obtained compounds **I**, **II** and **III** turned out to be contaminated with other technetium-containing product and were subjected to recrystallization from methanol. Approximate reaction yield by technetium: **I**, **II** = 50 %, **III** = 63%.

*3.2 Synthesis $[TcO_2(2\text{-}MeIm)_4]TcO_4$ (**IV**)*

9.5 mg of thiourea (Tu) and 5 μl of 2-methylimidazole (MeIm) were placed in a 1.5 ml vial and dissolved in 350 μl of methanol. 5 μl of 12M HCl and 10 μl of 3.5M $HTcO_4$ were added to the resulting solution. The intensely colored red solution was allowed to evaporate to dryness at room temperature (10 hours). Pink transparent crystals of **IV** were separated from the mother liquor and washed with methanol (20°C), the washings were

colorless. The resulting compound **IV** is less soluble in alcohols and acetone than those obtained **I**, **II**, **III**. Compound **IV** can be conveniently recrystallized from ethanol with the addition of 10% water. Approximate reaction yield by technetium 40%.

*3.3 Selection and synthesis (MeIm)(HMeIm)(Tu)TcO_4 (**V**)*

The alcohol solutions formed by washing the dry crystalline mixture of compound **IV** were evaporated by half at room temperature. Transparent colorless crystals formed along the meniscus of the liquid were selected for X-ray diffraction. An increase in the concentration of MeIm and a decrease in the acidity of the reaction mass leads to an increase in the content of compound V in the products (approx. 40-50% by Tc).

*3.4 Selection and synthesis HIm_2TcCl_6 (**VI**), Him_2TcBr_6 (**VII**) $(HMeIm)_4Tc/SnCl_6Cl_2$ (**VIII**)*

The methanolic solutions obtained after washing the mother crystalline mixtures of compounds **I**, **II** and **III** were mixed with the solutions obtained after recrystallization of the compounds obtained by method 2. After the slow evaporation of methanol, crystalline mixtures were obtained containing a small amount of compounds **I**, **II** and **III** (approx. 5 %), compounds **VI**, **VII** and **VIII** (approx. 30%). In a mixture containing compound **II**, the previously described [47] HImBr crystals were found.

Compounds **VI** and **VII** can be obtained analogously to the second synthesis method **I**, **II** and **III** by adding more HHal acid. Recrystallization of products **I**, **II**, and **III** from concentrated HHal acids also leads to the formation of hexahalotechnetates.

*3.5 Selection Tu_2Cl_2 (**IX**) and Tu_2Br_2 (**X**)*

In the dried crystalline mixture containing crystals of compounds **IV** and **V**, as well as in mixtures of compounds **I**, **II** and **III**, obtained by method 1, long transparent crystals of **IX** and **X** were found. They are readily soluble in methanol and can be purified from other impurities, including technetium compounds by recrystallization.

3.6 FTIR-Analysis

IR spectrum of the compound **II** was registered at Nicolet IR200 FT-IR from the 2 mg sample pressed as a finely grounded mixture with 100 mg KBr and pressed at 50 kg/sm^2.

3.7. Single-Crystal XRD Analysis

The crystal structure of all synthesized substances was determined by X-ray structural analysis using an automatic four-circle area-detector diffractometer Bruker KAPPA APEX II with MoKα radiation. The cell parameters were refined over the entire data set together with data reduction by using SAINT-Plus software [48]. Absorption corrections were introduced using the SADABS program [49]. The structures were solved by using the SHELXT-2018/2 program [50] and refined by full-matrix least squares on F^2 in the anisotropic approximation for all non-hydrogen atoms (SHELXL-2018/3 [51]). Atoms H, bounded to CH- and NH-groups, were placed in geometrically calculated positions with the isotropic temperature factors equal to 1.2 U_{eq}(C, N) and 1.5 U_{eq}(C) for CH_3-groups. The H atoms in water molecules in **I** were objectively located from the difference Fourier synthesis and refined with isotropic temperature factors equal 1.5 U_{eq}(O). The structure I was refined as inversion twin. Tables and figures for structures were generated using Olex2 [52].

Table 3. Crystal data and structure refinement for structures **II** – **VIII**.

Identification code	**II**	**III**	**IV**	**V**	**VI**	**VII**	**VIII**
Empirical formula	$C_{12}H_{20}BrN_8O_4Tc$	$C_{16}H_{28}ClN_8O_4Tc$	$C_{16}H_{24}N_8O_6Tc_2$	$C_9H_{17}N_6O_4STc$	$C_6H_{10}Cl_6N_4Tc$	$C_6H_{10}Br_6N_4Tc$	$C_{16}H_{28}Cl_8N_8Sn_{0.73}Tc_{0.27}$
Formula weight	518.27	529.91	620.43	403.34	448.88	715.64	729.22
Temperature/K	100 (2)				296 (2)		100 (2)
Crystal system	monoclinic	triclinic	monoclinic	monoclinic	monoclinic	monoclinic	monoclinic

Space group	*Cc*	*P*-1	*C*2/c	*P*2$_1$/*n*	C2/*m*	P2$_1$/c	*P*2$_1$/*c*
a/Å	13.0113(11)	8.2324(7)	14.8088(9)	10.5966(3)	12.4407(5)	7.6991(9)	14.7536(5)
b/Å	11.3064(9)	9.4890(8)	13.1343(8)	8.6220(3)	7.9932(4)	8.3979(9)	15.0790(5)
c/Å	14.2554(16)	15.2946(13)	12.9484(8)	17.2476(6)	7.4078(3)	12.8406(16)	13.4854(5)
α/°	90	107.160(3)	90	90	90	90	90
β/°	114.312(4)	95.947(3)	115.911(2)	94.804(1)	97.352(3)	98.166(7)	102.729(1)
γ/°	90	96.731(3)	90	90	90	90	90
Volume/Å^3	1911.1(3)	1121.63(17)	2265.3(2)	1570.27(9)	730.58(6)	821.81(17)	2926.36(18)
Z	4	2	4	4	2	2	4
ϱ_{calc}g/cm^3	1.801	1.569	1.819	1.706	2.041	2.892	1.655
μ/mm^{-1}	2.879	0.800	1.270	1.073	2.065	15.447	1.524
F(000)	1032.0	544.0	1240.0	816.0	438.0	654.0	1457.0
Crystal size/mm^3	0.4 × 0.12 × 0.1	0.3 × 0.27 × 0.25	0.18 × 0.1 × 0.06	0.36 × 0.22 × 0.18	0.4 × 0.23 × 0.19	0.22 × 0.12 × 0.1	0.18 × 0.12 × 0.1
Radiation	MoKα (λ = 0.71073)						
2Θ range for data collection/°	9.316 to 59.996	8.264 to 59.992	8.336 to 59.998	8.374 to 70	8.508 to 49.91	8.204 to 64.974	8.224 to 70
Index ranges	-15 ≤ h ≤ 18, -15 ≤ k ≤ 15, -20 ≤ l ≤ 20	-11 ≤ h ≤ 11, -13 ≤ k ≤ 11, -21 ≤ l ≤ 21	-20 ≤ h ≤ 20, -18 ≤ k ≤ 18, -18 ≤ l ≤ 18	-17 ≤ h ≤ 17, -13 ≤ k ≤ 13, -27 ≤ l ≤ 27	-14 ≤ h ≤ 14, -9 ≤ k ≤ 9, -8 ≤ l ≤ 8	-11 ≤ h ≤ 10, -12 ≤ k ≤ 12, -19 ≤ l ≤ 19	-23 ≤ h ≤ 21, -23 ≤ k ≤ 22, -21 ≤ l ≤ 21
Reflections collected	13375	19898	23979	72747	2927	18418	44345
Independent reflections	4644 [R_{int} = 0.0376, R_{sigma} = 0.0435]	6537 [R_{int} = 0.0425, R_{sigma} = 0.0557]	3283 [R_{int} = 0.0547, R_{sigma} = 0.0371]	6875 [R_{int} = 0.0488, R_{sigma} = 0.0254]	685 [R_{int} = 0.0336, R_{sigma} = 0.0279]	2960 [R_{int} = 0.0400, R_{sigma} = 0.0293]	12760 [R_{int} = 0.0370, R_{sigma} = 0.0389]
Data/restraints/parameters	4644/8/248	6537/0/281	3283/0/149	6875/0/192	685/30/58	2960/0/79	12760/0/315
Goodness-of-fit on *F*^{2}	1.030	1.039	1.049	1.051	1.065	1.052	1.020
Final R indexes [I>=2σ (I)]	R_1 = 0.0223, wR_2 = 0.0470	R_1 = 0.0487, wR_2 = 0.1090	R_1 = 0.0320, wR_2 = 0.0676	R_1 = 0.0238, wR_2 = 0.0510	R_1 = 0.0259, wR_2 = 0.0591	R_1 = 0.0415, wR_2 = 0.0877	R_1 = 0.0296, wR_2 = 0.0557
Final R indexes [all data]	R_1 = 0.0235, wR_2 = 0.0474	R_1 = 0.0665, wR_2 = 0.1204	R_1 = 0.0444, wR_2 = 0.0729	R_1 = 0.0310, wR_2 = 0.0539	R_1 = 0.0306, wR_2 = 0.0612	R_1 = 0.0665, wR_2 = 0.0966	R_1 = 0.0477, wR_2 = 0.0605
Largest diff. peak/hole / e Å^{-3}	0.34/-0.37	3.81/-1.88	0.65/-0.90	0.59/-0.51	0.47/-0.46	1.76/-1.03	1.50/-0.51
Flack parameter	0.588(7)						

Crystal data, data collection, and structure refinement details are summarized in Table 3. All other crystallographic parameters of the structures are indicated in Tables S1–S29. The atomic coordinates were deposited at the Cambridge Crystallographic Data Centre [53], CCDC № 1022420, 2193592-2193597 for **II** – **VIII**. The Supplementary crystallographic data can be obtained free of charge from the Cambridge Crystallographic Data Centre via www.ccdc.cam.ac.uk/data_request/cif (accessed on 30 July 2022).

4. Conclusions

In this work, we proposed two new methods for the preparation of $[TcO_2L_4]^+$ complexes (where L = imidazole (Im), methylimidazole (MeIm)). The reduction of Tc(VII) in an acidic alcoholic solution with thiourea leads to the selective formation of Tc(V). In the absence of a reducing agent, a complex salt Tc(VII) is formed. The reduction of Tc(VII) in an acidic aqueous solution by Sn(II) leads to the formation of a mixture of Tc(V) and Tc(IV) complexes. In a large excess of the reducing agent, Tc(IV) hexahalides are formed and the formation of double, mixed salt $(HMeIm)_4[Tc/SnCl_6]Cl_2$ is possible. The main by-products of the reactions are determined and the possible reaction mechanisms are considered. We have shown that Tc(VII) reduction by thiourea occurs via Tc(III) intermediates followed by oxidation to Tc(V).

The definition of the $[TcO_2Im_4]Br{\cdot}2H_2O$ crystal structure in non-centrosymmetric space group suggests that the literature description of the $[TcO_2Im_4]Cl{\cdot}2H_2O$ structure in the C2/c space group with disordered Cl and water positions may be erroneous. The lengths of the Tc-N and Tc=O bonds in complexes of the $[TcO_2L_4]^+$ type have been refined. Comparative analysis of non-valent interactions in the obtained crystals showed that with an increase in the size of the anion or the change of Im for MeIm the intermolecular interactions become weaker. In all the compounds obtained, except for $[TcO_2(MeIm)_4]TcO_4$, there are π-stacking interactions between aromatic rings. Halogen bonds and anion-π interactions have also been found in hexahalide-containing compounds. An analysis of the Hirshfeld surface showed that the main contribution to the crystal packing is made by van der Waals interactions of the type H···H (42.5–55.1%), H···C/C···H (17.7–21.3%) and hydrogen bonds, which contribute 15.7–25.3% in total.

Supplementary Materials: The following supporting information can be downloaded at: www.mdpi.com/xxx/s1, Table S1: Bond Lengths for **II** at 100 K, Table S2: Bond Angles for **II** at 100K, Table S3: Hydrogen Bonds for **II** at 100K, Table S4: Torsion Angles for **II** at 100 K Table S5: Bond Lengths for **III** at 100 K. Table S6: Bond Angles for **III** at 100 K. Table S7: Hydrogen Bonds for **III** at 100 K. Table S8: Torsion Angles for **III** at 100 K. Table S9: Bond Lengths for **IV** at 100 K. Table S10: Bond Angles for **IV** at 100 K. Table S11: Hydrogen Bonds for **IV** at 100 K Table S12: Torsion Angles for **IV** at 100 K. Table S13: Bond Lengths for **V** at 100 K. Table S14: Bond Angles for **V** at 100 K. Table S15: Hydrogen Bonds for **V** at 100 K. Table S16: Torsion Angles for **V** at 100 K. Table S17: Bond Lengths for **VI** at 296 K. Table S18: Bond Angles for **VI** at 296 K. Table S19: Hydrogen Bonds for **VI** at 296 K. Table S20: Torsion Angles for **VI** at 296 K. Table S21: Atomic Occupancy for **VI** at 296 K. Table S2: Table S22: Bond Lengths for **VII** at 296 K. Table S23: Bond Angles for **VII** at 296 K. Table S24: Hydrogen Bonds for **VII** at 296 K. Table S25: Torsion Angles for **VII** at 296 K. Table S26: Bond Lengths for **VIII** at 100 K. Table S27: Bond Angles for **VIII** at 100 K. Table S28: Hydrogen Bonds for **VIII** at 100 K Table S29: Torsion Angles for **VIII** at 100 K.

Author Contributions: For research articles with several authors, a short paragraph specifying their individual contributions must be provided. The following statements should be used "Conceptualization, A.P. Novikov and Volkov M.A; methodology, Fedoseev M.A. and Volkov M.A; software, A.P. Novikov; validation, A.P. Novikov, Volkov M.A and Guerman K. E.; formal analysis, A.P. Novikov; investigation, A.P. Novikov and Volkov M.A; resources, M.S. Grigoriev.; data curation, M.S. Grigoriev; writing—original draft preparation, Volkov M.A; writing—review and editing, Volkov M.A and A.P. Novikov; visualization, Volkov M.A and A.P. Novikov; supervision, Guerman K. E.; project administration, Guerman K. E.; funding acquisition, Guerman K. E. All authors have read and agreed to the published version of the manuscript." Please turn to the CRediT taxonomy for the term explanation. Authorship must be limited to those who have contributed substantially to the work reported.

Funding: The study was supported by the Ministry of Science and Higher Education of the Russian Federation (program no. 122011300061-3).

Institutional Review Board Statement: Not applicable.

Informed Consent Statement: Not applicable.

Acknowledgments: X-ray diffraction experiments were performed at the Center for Shared Use of Physical Methods of Investigation at the Frumkin Institute of Physical Chemistry and Electrochemistry,RAS.

Conflicts of Interest The authors declare no conflict of interest.

References

1. Volkov; Fedoseev; Krivoborodov, E.G.; Toropygin, I.Y.; German, E.; Grigoriev, S.; Kuznetsov, V. V.; Budantseva, N.; Novikov, P.; Mezhuev, Y.O. A new method for the synthesis of polynuclear carboxylate complexes of technetium (II, III). *J. Organomet. Chem.* **2022**, *957*, 122146, doi:10.1016/J.JORGANCHEM.2021.122146.
2. Alberto, R. From oxo to carbonyl and arene complexes; A journey through technetium chemistry. *J. Organomet. Chem.* **2018**, *869*, 264–269, doi:10.1016/J.JORGANCHEM.2018.01.013.
3. Sidorenko, G. V.; Miroslavov, A.E. Higher Technetium(I) Carbonyls and Possibility of Using Them in Nuclear Medicine: Problems and Prospects. *Radiochemistry* **2021**, *63*, 253–262, doi:10.1134/S1066362221030012.
4. Zegke, M.; Grödler, D.; Roca Jungfer, M.; Haseloer, A.; Kreuter, M.; Neudörfl, J.M.; Sittel, T.; James, C.M.; Rothe, J.; Altmaier, M.; et al. Ammonium Pertechnetate in Mixtures of Trifluoromethanesulfonic Acid and Trifluoromethanesulfonic Anhydride. *Angew. Chemie Int. Ed.* **2022**, *61*, e202113777, doi:10.1002/ANIE.202113777.
5. German, K.E.; Fedoseev, A.M.; Grigoriev, M.S.; Kirakosyan, G.A.; Dumas, T.; Den Auwer, C.; Moisy, P.; Lawler, K. V.; Forster, P.M.; Poineau, F. A 70-Year-Old Mystery in Technetium Chemistry Explained by the New Technetium Polyoxometalate [H7O3]4[Tc20O68] · 4H2O. *Chem. – A Eur. J.* **2021**, *27*, 13624–13631, doi:10.1002/CHEM.202102035.
6. Abram, U.; Beyer, R.; Münze, R.; Stach, J.; Kaden, L.; Lorenz, B.; Findeisen, M. Mixed-ligand complexes of technetium-III. Synthesis and characterization of [bis(diphenylphosphino)ethane]tetrakis(trimethylphosphite)technetium(I) hexafluorophosphate, [Tc(DPPE)(TMP)4]PF6. *Polyhedron* **1989**, *8*, 1201–1204, doi:10.1016/S0277-5387(00)81140-7.
7. Duatti, A. Review on 99mTc radiopharmaceuticals with emphasis on new advancements. *Nucl. Med. Biol.* **2021**, *92*, 202–216, doi:10.1016/J.NUCMEDBIO.2020.05.005.
8. Jürgens, S.; Herrmann, W.A.; Kühn, F.E. Rhenium and technetium based radiopharmaceuticals: Development and recent advances. *J. Organomet. Chem.* **2014**, *751*, 83–89, doi:10.1016/J.JORGANCHEM.2013.07.042.
9. Melent'ev, A.B.; Mashkin, A.N.; German, K.E. The influence of deviations in process parameters on the purification of uranium from different radionuclides. *Theor. Found. Chem. Eng. 2016 504* **2016**, *50*, 554–561, doi:10.1134/S0040579516040205.
10. Daolio, A.; Pizzi, A.; Terraneo, G.; Frontera, A.; Resnati, G. Anion···Anion Interactions Involving σ-Holes of Perrhenate, Pertechnetate and Permanganate Anions. *ChemPhysChem* **2021**, *22*, 2281–2285, doi:10.1002/cphc.202100681.
11. Xie, R.; Shen, N.; Chen, X.; Li, J.; Wang, Y.; Zhang, C.; Xiao, C.; Chai, Z.; Wang, S. 99TcO4-Separation through Selective Crystallization Assisted by Polydentate Benzene-Aminoguanidinium Ligands. *Inorg. Chem.* **2021**, *60*, 6463–6471, doi:10.1021/ACS.INORGCHEM.1C00187.
12. Zhu, L.; Sheng, D.; Xu, C.; Dai, X.; Silver, M.A.; Li, J.; Li, P.; Wang, Y.; Wang, Y.; Chen, L.; et al. Identifying the Recognition Site for Selective Trapping of 99TcO4- in a Hydrolytically Stable and Radiation Resistant Cationic Metal-Organic Framework. *J. Am. Chem. Soc.* **2017**, *139*, 14873–14876, doi:10.1021/JACS.7B08632.
13. Zhu, L.; Xiao, C.; Dai, X.; Li, J.; Gui, D.; Sheng, D.; Chen, L.; Zhou, R.; Chai, Z.; Albrecht-Schmitt, T.E.; et al. Exceptional perrhenate/pertechnetate uptake and subsequent immobilization by a low-dimensional cationic coordination polymer: Overcoming the hofmeister bias selectivity. *Environ. Sci. Technol. Lett.* **2017**, *4*, 316–322, doi:10.1021/ACS.ESTLETT.7B00165.
14. Sheng, D.; Zhu, L.; Dai, X.; Xu, C.; Li, P.; Pearce, C.I.; Xiao, C.; Chen, J.; Zhou, R.; Duan, T.; et al. Successful Decontamination of 99TcO4− in Groundwater at Legacy Nuclear Sites by a Cationic Metal-Organic Framework with Hydrophobic Pockets. *Angew. Chemie* **2019**, *131*, 5022–5026, doi:10.1002/ANGE.201814640.
15. Chotkowski, M.; Wrzosek, B.; Grdeń, M. Intermediate oxidation states of technetium in concentrated sulfuric acid solutions.

J. Electroanal. Chem. **2018**, *814*, 83–90, doi:10.1016/J.JELECHEM.2018.02.042.

16. Li, J.; Li, B.; Shen, N.; Chen, L.; Guo, Q.; Chen, L.; He, L.; Dai, X.; Chai, Z.; Wang, S. Task-Specific Tailored Cationic Polymeric Network with High Base-Resistance for Unprecedented 99TcO4-Cleanup from Alkaline Nuclear Waste. *ACS Cent. Sci.* **2021**, *7*, 1441–1450, doi:10.1021/ACSCENTSCI.1C00847.
17. Fackler, P.H.; Lindsay, M.J.; Clarke, M.J.; Kastner, M.E. Synthesis and structure of trans-[O2(Im)4Tc]Cl·2H2O, trans-[O2(1-meIm)4Tc]Cl·3H2O and related compounds. *Inorganica Chim. Acta* **1985**, *109*, 39–49, doi:10.1016/S0020-1693(00)86325-2.
18. Louis-Jean, J.; George, J.; Poineau, F. From ammonium Hexahalorhenates(IV) to nanocrystalline rhenium metal: A combined thermal, diffraction and microscopic analysis. *Int. J. Refract. Met. Hard Mater.* **2022**, *105*, 105840, doi:10.1016/J.IJRMHM.2022.105840.
19. Louis-Jean, J.; Swift, A.J.; Hatchett, D.W.; Poineau, F. Conversion of (NH4)2[ReF6] into ReO2 mixed phases: A thermal analysis study. *Inorg. Chem. Commun.* **2022**, *140*, 109482, doi:10.1016/J.INOCHE.2022.109482.
20. Baldas, J.; Colmanet, S.F.; Ivanov, Z.; Williams, G.A. Preparation and structure of [{Tc V N(thiourea)} 4 (edta) 2]·6H 2 O: the first example of a cyclic nitrido-bridged tetrameric technetium complex. *J. Chem. Soc. Chem. Commun.* **1994**, *0*, 2153–2154, doi:10.1039/C39940002153.
21. Abrams, M.J.; Davison, A.; Faggiani, R.; Jones, A.G.; Lock, C.J.L. Chemistry and Structure of Hexakis (thiourea-S) technetium (III) Trichloride Tetrahydrate, [Tc(SC(NH2)2)6]Cl3.4H2O. *Inorg. Chem.* **1984**, *23*, 3284–3288, doi:10.1021/ic00189a003.
22. Omori, T. Substitution reactions of technetium compounds. In *Technetium and Rhenium Their Chemistry and Its Applications*; Yoshihara, K., Omori, T., Eds.; Springer Berlin Heidelberg: Berlin, Heidelberg, 1996; pp. 253–273 ISBN 978-3-540-49273-3.
23. Welch, M.J.; Redvanly, C.S. *Handbook of radiopharmaceuticals : radiochemistry and applications*; J. Wiley, 2003; ISBN 978-0-470-84638-4.
24. Abram, U.; Alberto, R. Technetium and rhenium: coordination chemistry and nuclear medical applications. *J. Braz. Chem. Soc.* **2006**, *17*, 1486–1500, doi:10.1590/S0103-50532006000800004.
25. Liu, S. The role of coordination chemistry in the development of target-specific radiopharmaceuticals. *Chem. Soc. Rev.* **2004**, *33*, 445–461, doi:10.1039/B309961J.
26. Maruk, A.Y.; Bruskin, A.B.; Kodina, G.E. Novel 99m Tc radiopharmaceuticals with bifunctional chelating agents. *Radiochemistry* **2011**, *53*, 341–353, doi:10.1134/S1066362211040011.
27. Sergienko, V.S.; Churakov, A. V. Specific features of technetium mononuclear octahedral oxo complexes: A review. *Crystallogr. Reports* **2013**, *58*, 1–25, doi:10.1134/S1063774513010112.
28. Novikov, A.P.; Volkov, M.A.; Safonov, A.V.; Grigoriev, M.S. Synthesis, Crystal Structure, and Hirshfeld Surface Analysis of Hexachloroplatinate and Tetraclorouranylate of 3-Carboxypyridinium—Halogen Bonds and π-Interactions vs. Hydrogen Bonds. *Crystals* **2022**, *12*, 271, doi:10.3390/cryst12020271.
29. Alvarez, S. A cartography of the van der Waals territories. *Dalt. Trans.* **2013**, *42*, 8617–8636, doi:10.1039/C3DT50599E.
30. Novikov, A.P.; Volkov, M.A.; Safonov, A.V.; Grigoriev, M.S.; Abkhalimov, E.V. Synthesis and Characterization of New Guanine Complexes of Pt(IV) and Pd(II) by X-Ray Diffraction and Hirshfeld Surface Analysis. *Crystals* **2021**, *11*, 1417, doi:10.3390/CRYST11111417.
31. Savastano, M.; García, C.; López de la Torre, M.D.; Pichierri, F.; Bazzicalupi, C.; Bianchi, A.; Melguizo, M. Interplay between salt bridge, hydrogen bond and anion-π interactions in thiocyanate binding. *Inorganica Chim. Acta* **2018**, *470*, 133–138, doi:10.1016/J.ICA.2017.04.029.
32. Bombicz, P.; Mutikainen, I.; Krunks, M.; Leskelä, T.; Madarász, J.; Niinistö, L. Synthesis, vibrational spectra and X-ray structures of copper(I) thiourea complexes. *Inorganica Chim. Acta* **2004**, *357*, 513–525, doi:10.1016/J.ICA.2003.08.019.
33. Spackman, M.A.; Jayatilaka, D. Hirshfeld surface analysis. *CrystEngComm* **2009**, *11*, 19–32, doi:10.1039/b818330a.
34. Piña, J.J.; Gil, D.M.; Pérez, H. Revealing new non-covalent interactions in polymorphs and hydrates of Acyclovir: Hirshfeld

surface analysis, NCI plots and energetic calculations. *Comput. Theor. Chem.* **2021**, *1197*, 113133, doi:10.1016/J.COMPTC.2020.113133.

35. Marek, P.H.; Urban, M.; Madura, I.D. The study of interactions with a halogen atom: influence of NH2 group insertion on the crystal structures of meta-bromonitrobenzene derivatives. *Acta Crystallogr. Sect. C Struct. Chem.* **2018**, *74*, 1509–1517, doi:10.1107/S2053229618013608.
36. Novikov, A.P.; Bezdomnikov, A.A.; Grigoriev, M.S.; German, K.E. Synthesis, crystal structure and Hirshfeld surface analysis of 2-(perfluorophenyl)acetamide in comparison with some related compounds. *Acta Crystallogr. Sect. E Crystallogr. Commun.* **2022**, *78*, 80–83, doi:10.1107/S2056989021013359.
37. Psycharis, V.; Dermitzaki, D.; Raptopoulou, C.P. The Use of Hirshfeld Surface Analysis Tools to Study the Intermolecular Interactions in Single Molecule Magnets. *Cryst. 2021, Vol. 11, Page 1246* **2021**, *11*, 1246, doi:10.3390/CRYST11101246.
38. Tan, S.L.; Jotani, M.M.; Tiekink, E.R.T. Utilizing Hirshfeld surface calculations, non-covalent inter-action (NCI) plots and the calculation of inter-action energies in the analysis of mol-ecular packing. *Acta Crystallogr. Sect. E Crystallogr. Commun.* **2019**, *75*, 308–318, doi:10.1107/S2056989019001129.
39. Spackman, P.R.; Turner, M.J.; McKinnon, J.J.; Wolff, S.K.; Grimwood, D.J.; Jayatilaka, D.; Spackman, M.A. CrystalExplorer : a program for Hirshfeld surface analysis, visualization and quantitative analysis of molecular crystals. *J. Appl. Crystallogr.* **2021**, *54*, 1006–1011, doi:10.1107/S1600576721002910.
40. Du Preez, J.G.H.; Gerber, T.I.A.; Fourie, P.J.; Van Wyk, A.J. The Chemistry of rhenium and technetium. Part 1. Syntheses and characterisation of new dioxo technetium(V) complexes with schiff base type ligands. *Inorganica Chim. Acta* **1984**, *82*, 201–205, doi:10.1016/S0020-1693(00)82492-5.
41. Kastner, M.E.; Lindsay, M.J.; Clarke, M.J. Synthesis and Structure of trans-[O2(en)2Tcv]+. *Inorg. Chem.* **1982**, *21*, 2037–2040, doi:10.1021/ic00135a062.
42. Zuckman, S.A.; Freeman, G.M.; Troutner, D.E.; Volkert, W.A.; Holmes, R.A.; Van Derveer, D.G.; Barefield, E.K. Preparation and X-ray Structure of trans-Dioxo(1,4,8,11-tetraazacyclotetradecane)technetium(V) Perchlorate Hydrate. *Inorg. Chem.* **1981**, *20*, 2386–2389, doi:10.1021/ic50222a006.
43. Bykov, A. V.; Starokurov, Y. V.; Saletsky, A.M. IR Spectroscopy of Bidistilled and Deuterium Water under Conditions of Geometric Limitation in Glass Nanopores. *Opt. Spectrosc.* **2020**, *128*, 114–118, doi:10.1134/S0030400X20010063.
44. Wang, X.; Wang, D.; Guo, Y.; Yang, C.; Iqbal, A.; Liu, W.; Qin, W.; Yan, D.; Guo, H. Imidazole derivative-functionalized carbon dots: using as a fluorescent probe for detecting water and imaging of live cells. *Dalt. Trans.* **2015**, *44*, 5547–5554, doi:10.1039/C5DT00128E.
45. 1H-Imidazole Available online: https://webbook.nist.gov/cgi/cbook.cgi?ID=C288324&Mask=80 (accessed on Jul 30, 2022).
46. *Handbook of Radioactivity Analysis: Volume 2. Radioanalytical applications.*; L'Annunziata, M.F., Ed.; 2020; ISBN 978-0-12-814395-7.
47. Ggor, A.; Piecha, A.; Jakubas, R.; Miniewicz, A. Crystal structure and characterization of a novel acentric imidazolium analog [C3N2H5+][Br-]. *Chem. Phys. Lett.* **2011**, *503*, 134–138, doi:10.1016/J.CPLETT.2010.12.083.
48. Bruker AXS Inc.: Madison, WI, U. SAINT, V8.40B 2020.
49. Krause, L.; Herbst-Irmer, R.; Sheldrick, G.M.; Stalke, D. Comparison of silver and molybdenum microfocus X-ray sources for single-crystal structure determination. *J. Appl. Crystallogr.* **2015**, *48*, 3–10, doi:10.1107/S1600576714022985.
50. Sheldrick, G.M. SHELXT - Integrated space-group and crystal-structure determination. *Acta Crystallogr. Sect. A Found. Crystallogr.* **2015**, *71*, 3–8, doi:10.1107/S2053273314026370.
51. Sheldrick, G.M. Crystal structure refinement with SHELXL. *Acta Crystallogr. Sect. C Struct. Chem.* **2015**, *71*, 3–8, doi:10.1107/S2053229614024218.
52. Dolomanov, O. V.; Bourhis, L.J.; Gildea, R.J.; Howard, J.A.K.; Puschmann, H. OLEX2: A complete structure solution,

refinement and analysis program. *J. Appl. Crystallogr.* **2009**, *42*, 339–341, doi:10.1107/S0021889808042726.

53. Groom, C.R.; Bruno, I.J.; Lightfoot, M.P.; Ward, S.C. The Cambridge Structural Database. *Acta Crystallogr. Sect. B Struct. Sci. Cryst. Eng. Mater.* **2016**, *72*, 171–179, doi:10.1107/S2052520616003954.